FUSION SCIENCE AND TECHNOLOGY · VOLUME 75 · 664–673 · OCTOBER 2019

DOI: https://doi.org/10.1080/15361055.2019.1646608

Plasma-Material-Interaction Research Using PISCES Linear Plasma Devices

M. J. Baldwin,* R. P. Doerner, D. Nishijima, M. Patino, M. J. Simmonds, G. Tynan, J. H. Yu, and A. Založnik

University of California at San Diego,Center for Energy Research, San Diego, California 92093-0417

Received June 14, 2018
Accepted for Publication July 18, 2019

Abstract — *Recent plasma-material-interaction (PMI) studies of relevance to fusion PMI science are discussed. The results are a mix of science experiments and in situ diagnostic technology development. Scientific issues addressed include the nature of He and W atom migration in the evolution of W fuzz surfaces, understanding the nature of D retention in damaged W surfaces via modeling with the tritium migration and analysis program, and an examination of synergistic effects associated with D trapping on composite Be codeposit and W substrate surfaces. In situ diagnostic developments discussed include laser-induced desorption spectroscopy for the measurement of bulk hydrogen retention and laser-induced breakdown spectroscopy for the measurement of near-surface composition.*

Keywords — *Plasma-material interaction, beryllium, tungsten, ITER, tritium migration and analysis program, laser-induced desorption spectroscopy, laser-induced breakdown spectroscopy.*

Note — *Some figures may be in color only in the electronic version.*

I. INTRODUCTION

Understanding the scientific and technical challenges associated with plasma-material interaction (PMI) and edge and scrape-off layer (SOL) boundary plasma is crucial for developing plasma-facing components (PFCs) for current and next-step magnetic fusion energy systems.[1] In these systems, the use of multimaterial PFC designs leads to SOL PMI and transport processes that give rise to the formation of mixed materials on both the divertor and main plasma PFCs. The performance and interaction of these mixed materials with the plasma during steady-state, transient, and off-normal plasma events then, in turn, play a critical role in determining PFC lifetime, tritium fuel retention, and plasma performance.

For over 30 years, the Plasma Interaction with Surface Component Experiment (PISCES) research program at the University of California at San Diego (UCSD) has performed PMI and boundary plasma science studies with a view toward prediction and optimization of PFC performance. Most of the research is carried out on the linear plasma devices (LPDs) PISCES-A (Ref. 2) and PISCES-B (Ref. 3), which are steady-state flowing plasma systems capable of producing energetic (H, D, He) ion bombardment fluxes in the range of 10^{21} to 10^{23} $m^{-2}{\cdot}s^{-1}$ on fusion-relevant material targets at impact energies up to several hundred electron volts. The PISCES-A LPD is a multipurpose system that hosts a number of experimental activities spanning material exposure to plasma transport studies, while the PISCES-B LPD is tasked more specifically with ITER-relevant research experiments involving the use of beryllium.[4] The program also takes advantage of a number of other laboratory plasma devices, laser-based systems, and diagnostic apparatus to support its research mission with brief descriptions given throughout the paper as necessary. The following is a summary of recent key PISCES experimental results and diagnostic developments that were presented at the 23rd TOFE topical meeting.

*E-mail: m1baldwin@.ucsd.edu

II. THE DYNAMICS OF HE AND W ATOMS IN W FUZZ

Fuzz manifests as the growth of a surface layer of nanoscopic tendrils and has been documented for a wide variety of materials upon exposure to He plasma within a specific material-dependent temperature window.[5] Most studies of the fuzz effect have been carried out for tungsten because of its importance as a candidate nuclear fusion material. However, in spite of more than a decade of research on fuzz (for example, Ref. 5 and references therein), there remains no complete understanding on the precise mechanisms and processes that lead to fuzz formation, with the exception of agreement that the process is strongly linked to subsurface He precipitation in the form of nanobubbles. The experiments described in this section focus on the dynamic behavior in which He fills such nanobubbles as well the motion of W atoms during fuzz formation, with the findings providing new insight into aspects of the fuzz formation process. Complete details are to be found in Ref. 6.

A series of plasma exposures in mixtures of ^{3}He-^{4}He and ^{4}He, on W, were carried out using the PISCES-A LPD at a temperature of ~1100 K and a flux of 3×10^{22} to 5×10^{22} $m^{-2} \cdot s^{-1}$, with an associated ion impact energy of ~55 eV achieved by application of a negative bias to the W target. The impact energy is chosen to be well below the sputter threshold of the W, which is ~120 eV for ^{4}He. Following exposure, the ^{3}He content in the target is quantified by nuclear reaction analysis (NRA) utilizing the ^{3}He(D,p)^{4}He reaction with an analysis depth of ~2 μm. To examine the motion of He atoms during the formation of tungsten fuzz, ^{3}He was injected into the plasma at various admixture values of up to 25% at different stages of the plasma exposure. Following exposure, NRA measurements were made across the face of the target. On each target face the fuzz was removed from one side (by wiping) to examine the ^{3}He content below the fuzz layer, while on the other side the fuzz was left intact to measure the ^{3}He in the fuzz layer as well. The arrangement is shown pictorially in Fig. 1, in addition to NRA data from four different target samples. Figure 1a shows the ^{3}He content across the sample face for a ^{3}He (25%)–^{4}He plasma exposure of 60-min duration. A surprising result is that a significant level (~80%) of the ^{3}He is determined to be in the substrate under the fuzz. Figure 1b shows the result for a 90-min plasma exposure where ^{3}He(10%) was added to the plasma in the final 30 min on an already well-developed fuzz layer. As with the first case, the fact that ^{3}He is found in the substrate suggests that the fuzz is somewhat transparent to He ions since the ^{3}He was injected into the plasma at the end of the discharge. Figure 1c shows the result for a 90-min plasma exposure where ^{3}He(5%) was added to the plasma only during the initial 30 min. A null result (i.e., no ^{3}He detected) indicates that the initial ^{3}He was not trapped or frozen into the nanobubbles but escaped during the remainder of the discharge with just ^{4}He, and the escape occurred in spite of a 6- to 9-eV surface barrier for He to penetrate the bubble inner W surface.[7] Last, Fig. 1d shows results for a 90-min plasma exposure where ^{3}He(5%) was added to the plasma only during the final 5 min. In this test the ratio of the ^{3}He ion fluence to the target compared with that of Fig. 1b was ~0.05, which is very close to the ratio of the amounts of ^{3}He detected. The total He ion fluence was similar in each case implying that the trapping of He in the W is proportional to the ion bombardment fluence.

In a second experiment, 15 nm of isotopically enriched tungsten (~92.99% ^{182}W) was deposited on the surface of a bulk tungsten sample of naturally occurring isotopic abundance. This sample was then exposed at 1150 K to He plasma for a duration of 1 h to produce a fuzz surface layer. Secondary ion mass spectrometry (SIMS) was used before and after the plasma exposure to track the motion of the isotopes. The SIMS depth profiles are shown in Fig. 2 and reveal strong mixing of the tungsten atoms from the substrate and isotopically enriched layer during the fuzz formation process.

Collectively, the results of both experiments suggest that W fuzz formation involves dynamic processes involving continuous He uptake, He release, and W atom motion in both the substrate and fuzz tendril material. A further conclusion of this work is that a driving mechanism in He fuzz growth, being the trapping of He, is not limited by He diffusion as this would require He trapping at a rate proportional to the square root of the ion fluence. This should not however be confused with the measure of fuzz layer thickness, which does grow with the square root of the ion fluence.[8]

III. ADAPTING TMAP FOR THE STUDY OF D RETENTION IN DAMAGED W SURFACES

As we move toward burning plasma regimes such as will be apparent in ITER, the effects of neutron damage on materials is under increasing focus in PISCES PMI research. To examine such effects, heavy-ion beams of several mega-electron-volts (e.g.,

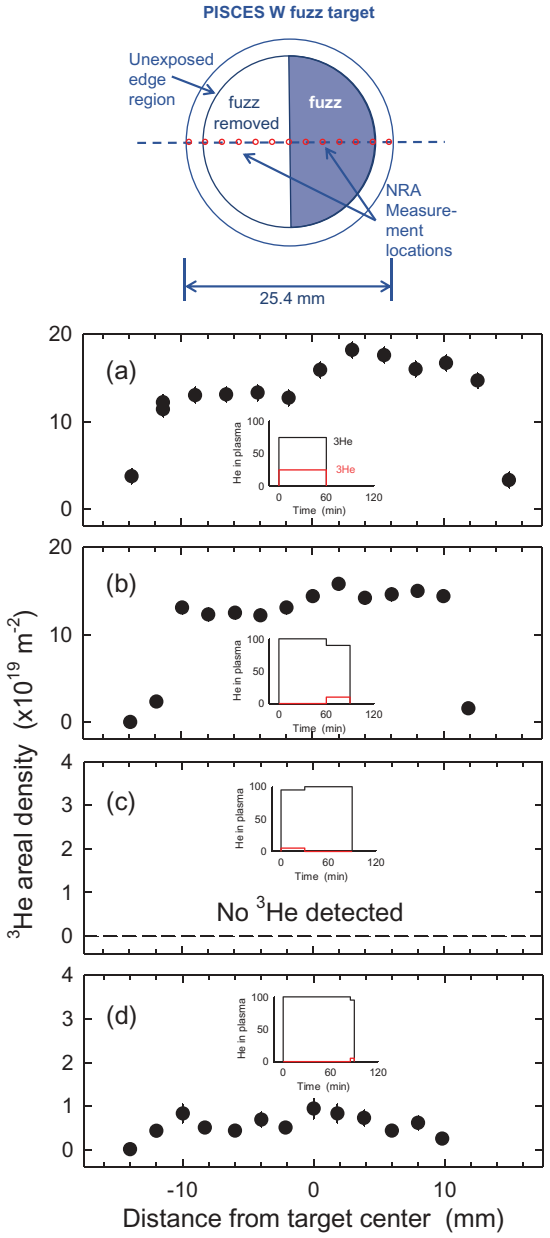

Fig. 1. NRA line scan measurements of areal D retention across W targets exposed to mixtures of ^{3}He-^{4}He and ^{4}He plasmas at ~1100 K. The schematic demonstrates the orientation of fuzz removal by wiping. Insets describe ^{3}He admixture timing to the ^{4}He plasma at various stages of the exposure: (a) ^{3}He(25%) added for the duration of a 60-min exposure, (b) ^{3}He(10%) added in the final 30 min of a 90-min exposure, (c) ^{3}He(5%) added in the initial 30 min of a 90-min exposure, and (d) ^{3}He(5%) added during the final 5 min of a 90-min exposure.

W or Cu) are typically used to produce damage in the near surface (below 10 μm) of targets. Such ion beams do not damage the material in the same way as 14-MeV fusion neutrons, but at least, studies of damage-related influences on PMI can be studied. Here, a recent adaptation of the tritium migration and analysis program[9] (TMAP) is outlined in its application to studying the effect of damage on hydrogen isotope retention in, and release from, the material W.

A key measurement in the PISCES laboratory for studying hydrogen isotope retention and release is thermal desorption mass spectrometry (TDS). However, fully understanding TDS data is not usually straightforward and requires complex modeling of a coupled system of differential equations to infer information on trap concentrations and the trap release energies pertaining to the material system being studied. The TMAP code package is capable of performing the necessary computations and is well validated,[9] but at present, TMAP can only simulate material systems with up to a maximum of three distinct trap types characterized by a concentration distribution, and trap capture and releases rates. To overcome this limitation and extend to systems with greater numbers of different traps, a pseudo-trap and temperature partition (PTTP) scheme was developed.[10] In this scheme, traps that are actively trapping but inactively releasing at a specific temperature are lumped together as a single pseudo trap, thereby reducing the number of equations to be solved in an incremental temperature window and thus allowing for an increased number of different trap types to be simulated over a given temperature range. All of this is carried out using a MATLAB routine that iteratively manipulates the TMAP input file and continuously restarts the TMAP package to achieve a final simulation.

An example of the application of the pseudo-trap TMAP analysis is given in Fig. 3. Figure 3 shows TDS data for a sample of W (6-mm diameter, 1.5-mm thickness) that was damaged with 3.4-MeV Cu ions to a peak displacement-per-atom ratio of ~0.2 at a depth of 0.9 μm and then exposed to D_2 plasma in the PISCES-E radio-frequency (rf) LPD at 383 K to a fluence of 10^{24}-m^{-2} deuterium ions of ~110-eV energy. The TDS D release is found to be broad and occurs over a wide temperature range beginning at ~400 K and ending at ~1000 K due to the multiplicity of traps created by the heavy-ion damage. Figure 3 also shows a limited three-trap TMAP and a six-trap PTTP scheme TMAP simulation. The TMAP simulation with three-trap limitation utilizes traps of release energies of 1.1, 1.4, and 1.9 eV. However, the agreement is somewhat poor and displays an ~20% residual. When modeled with the adapted PTTP TMAP scheme and six traps of release energies of 0.9, 1.1, 1.4, 1.7, 1.9, and 2.1 eV,

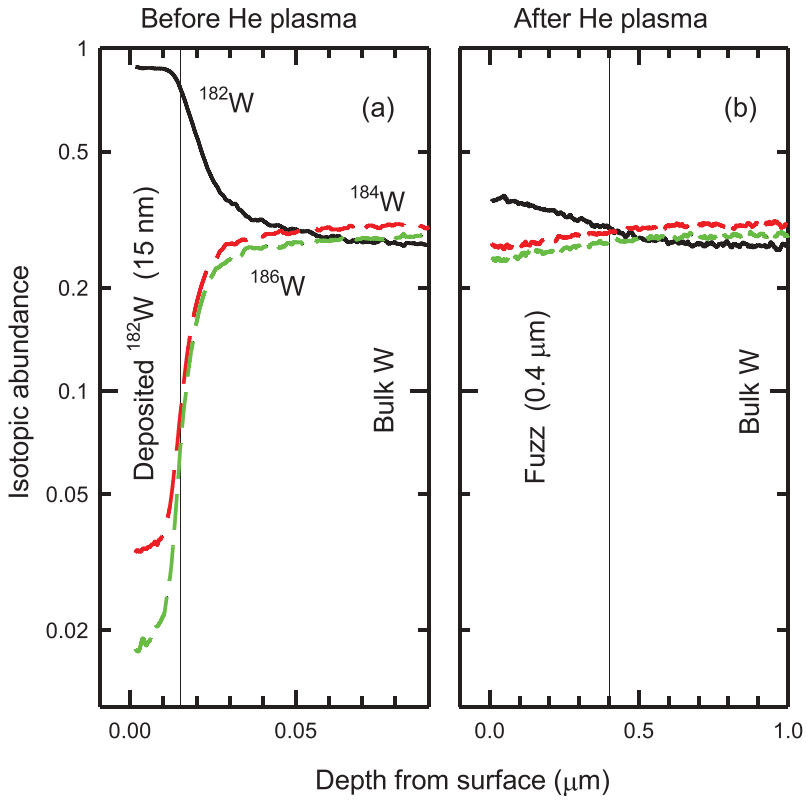

Fig. 2. SIMS depth profiles of (a) 15 nm of isotopically enriched ^{182}W deposited on a bulk W sample of natural isotopic abundance and (b) the same sample following exposure at 1150 K to He plasma for 1 h to produce a fuzz surface layer ~0.4 μm thick.

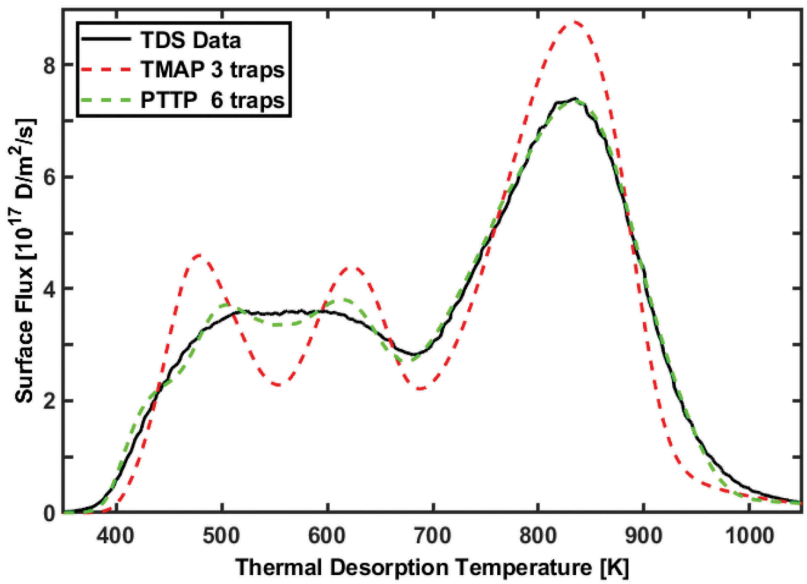

Fig. 3. An example of the application of pseudo-trap TMAP analysis to TDS data for D_2 plasma exposed damaged W. Two TMAP simulations are compared to the TDS data: a limited three-trap simulation with ~20% residual and a six-trap PTTP scheme (pseudo-trap) TMAP simulation with ~4% residual.

the agreement is significantly improved, and the residual is much better at only 4%. The development of the TMAP PTTP scheme has therefore increased the capability of TMAP in multitrap materials and TDS analysis and simulation. Complete details of this study are given in Ref. 10.

IV. SYNERGISTIC D TRAPPING EFFECTS IN COMPOSITE BE CODEPOSIT AND W SUBSTRATE SURFACES

A common model for retention of hydrogen isotopes in materials is that upon implantation the isotopes diffuse away from the surface and into the bulk, encountering and filling preexisting trap sites[9] and thereby forming a diffusion front that progresses into the material. For W, preexisting trap sites are typically assumed to vary from 10^{-5} to 10^{-3} per W atom based on measured hydrogen depth profiles,[11] and such values are typically required to model the hydrogen isotope uptake with a diffusion-reaction code like TMAP (Ref. 12). However, Gao et al.[13] have recently showed the existence of a 10-nm-thick D-supersaturated surface layer with a high D concentration of ~10 at. % after irradiation with low-energy ions and suggest a synergistic interaction of implanted D ions and solute D atoms with the W lattice. In their proposition, solute D atoms prevent the recombination of vacancies produced by lattice collisions with impinging D ions, with counterpart interstitial W atoms thus formed. The so-called Frenkel pairs then become further D trapping sites, thus driving a high D surface concentration (~0.1) that is much higher than accountable by intrinsic traps. Recent experiments in the PISCES laboratory show a similar result, with the exception that the mechanism observed is operative beyond the implantation zone. The results, which are arrived at through a combination of PMI and TDS experiments, and thermal release modeling with TMAP have strong implications for the way retention in W is understood and modeled.

In the experiment, two identically prepared W samples are exposed together at 560 K to deuterium plasma in the PISCES-A LPD, receiving a D ion fluence of 3×10^{25} m^{-2} and 80 eV. One of the samples is used as a control sample and analyzed using TDS to give the thermal release from the PMI W. The other PMI W sample is then coated, along with an unexposed W sample, with a layer (5 to 10 nm) of Be-D codeposits using a magnetron sputtering system.[14] Both of these samples are then analyzed with TDS to give the thermal release from the D_2 PMI W with the codeposit layer as well as the release from the codeposit only. The TDS results are then modeled with TMAP using prior developed models for D_2 PMI W (Ref. 12), and codeposited Be (Ref. 14).

The TDS data and TMAP modeling are shown in Fig. 4. The D_2 PMI W control TDS data show trap release at peaks ~700 K and 850 K. In comparison, the Be-D codeposit on unexposed W begins with a strong sharp release at ~490 K that diminishes at higher temperature. In the composite Be-D codeposit on the PMI W case, D released from the bulk W traps (~700 K and 850 K) is increased, but the increase matches a reduction in the low-temperature sharp release associated with the codeposit layer (~490 K). However, the areal density of D in the three samples is consistent according to the PMI and deposition processing of each. Collectively, an interpretation of all three TDS data sets is that during the TDS temperature ramp, the PMI bulk W pumps the Be-D codeposit overlayer, and that trapping in bulk W traps is increased by ~3 to 5 for the mobile D, which leaves the codeposit and diffuses into the PMI W.

The interpretation is explored by modeling the data with TMAP using desorption models built on prior work—a PMI W model is reported in Ref. 2, and a Be-D codeposit model is reported in Ref. 4—and to model the composite case of a Be-D layer with PMI W substrate only requires that the two models be coupled. Beginning with Fig. 4, the control D_2 PMI W release is simulated reasonably by two trap concentrations of 1.6×10^{-5} and 3.0×10^{-6} of release energies of 1.6 and 1.9 eV. Presumably, this gives information on the D trapping properties of the W used in the experiment. However, referring to Fig. 5, the TDS data for the Be-D codeposit layer on the unexposed W substrate are shown with three overlays of a combined TMAP simulation. The Be-D codeposit layer is simulated with two traps of release energies of 0.8 and 1.0 eV and the W substrate with the same preexisting traps of 1.6 and 1.9 eV determined from the control D_2 PMI W case. In the simulations the trap concentrations in the W ($W:C_t$) are increasingly varied as shown in Fig. 5. It is noted that increased substrate traps in the W lead to emergent high-temperature release peaks that are just not seen in the TDS data. The only conclusion is that the preexisting or intrinsic trap concentration in the non-plasma-exposed W substrate is below $\sim 2 \times 10^{-6}$. Yet, the TMAP model of Fig. 4 shows, subsequent to PMI, that the trap concentration in the D_2 PMI W is larger by an order of magnitude in order to simulate the TDS data. Taken together, the results suggest that traps are produced by the PMI. Further, in the composite case (D_2 PMI W plus codeposit) in Fig. 4, the TDS data are only reproduced by TMAP simulation if the concentrations of bulk W 1.6- and 1.9-eV traps in the near W surface (a few hundred nanometers) are increased further to 1.5×10^{-3} and 2.0×10^{-5}. That is, significantly more traps are necessary in the first 100 nm of the W substrate, with respect to the D_2 W PMI case, to give the observed pumping effect in the simulation that matches the experiment. Given the necessary 100-nm range required to model the effect and the use of a below sputter threshold ion energy for W displacement during the PMI, it is deduced that the extra trapping is not entirely related to

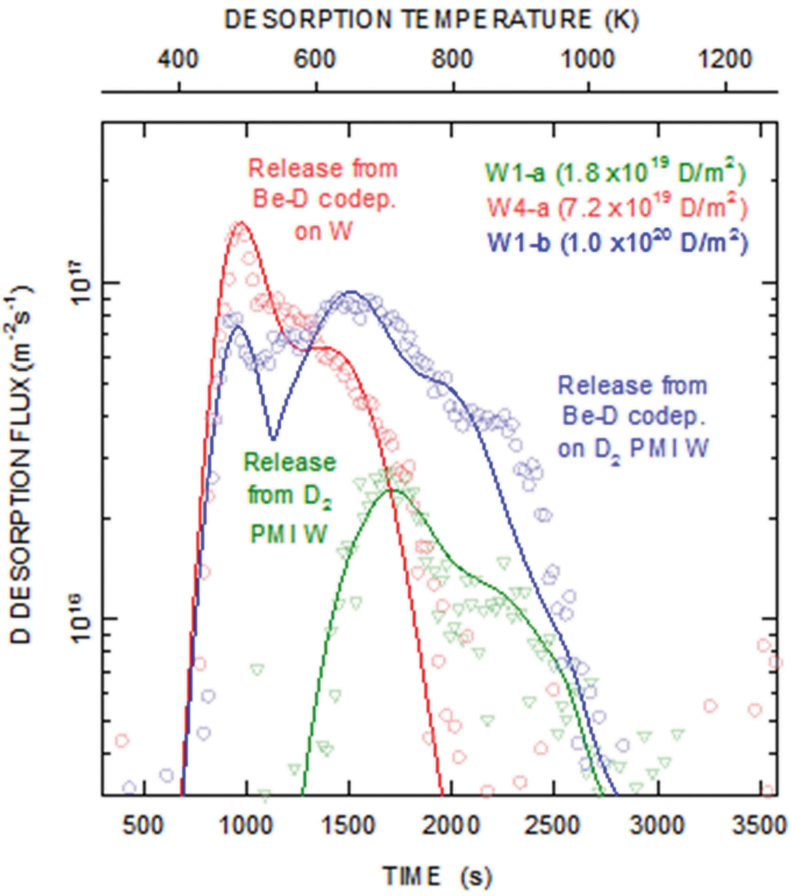

Fig. 4. TDS and TMAP simulations for three W PMI samples. Data are shown for a W sample exposed in PISCES-A at 560 K to D_2 plasma up to a fluence of 3×10^{25} m^{-2}, 80-eV deuterium ions; a second W sample exposed identically but with a 5- to 10-nm layer of sputtered Be-D codeposit; and a third W sample that was not exposed to plasma but is coated in an identical Be-D codeposit layer.

ion bombardment during the PMI as in Ref. 13 but to the presence of additional D in the surface region during the TDS desorption. That is, all of the data seem to suggest evidence of D concentration driven trap formation in W. The study of this effect is ongoing with further samples prepared and under examination using NRA to measure the D concentration depth profiles in the surface and validate the TMAP modeling.

V. LASER-INDUCED DESORPTION SPECTROSCOPY FOR TARGETED IN SITU D RETENTION MEASUREMENT AND REMOVAL

Tritium management will be a major factor in future fusion devices and will depend on the ability of the reactor to breed it. However, inefficiencies including tritium uptake in PFCs and codeposits are seen as a challenge to tritium self-sufficiency. Consequently, tritium inventory assessment and control in plasma-wetted surfaces is a priority scientific direction[1] in ongoing fusion research. The technique of laser-induced desorption spectroscopy (LIDS) is currently being explored in the PISCES laboratory as a technology development with the potential for targeted, in situ, hydrogen isotope measurement in and removal from PMI surfaces. Here, we summarize the initial results with the technique for the measurement and removal of D from Ti-D codeposited layers, which were chosen because of high D content and hence good signal detection in these proof-of-principle experiments. Full details of the system and results for W codeposited layers are to be published separately.[15]

A batch of Ti-D codeposit samples was produced at 500 K on 6-mm-diameter, 1.5-mm-thick nickel samples using a sputtering system. The codeposit layers were measured to be 4 μm thick according to the mass gain on each sample. One sample was analyzed for D content

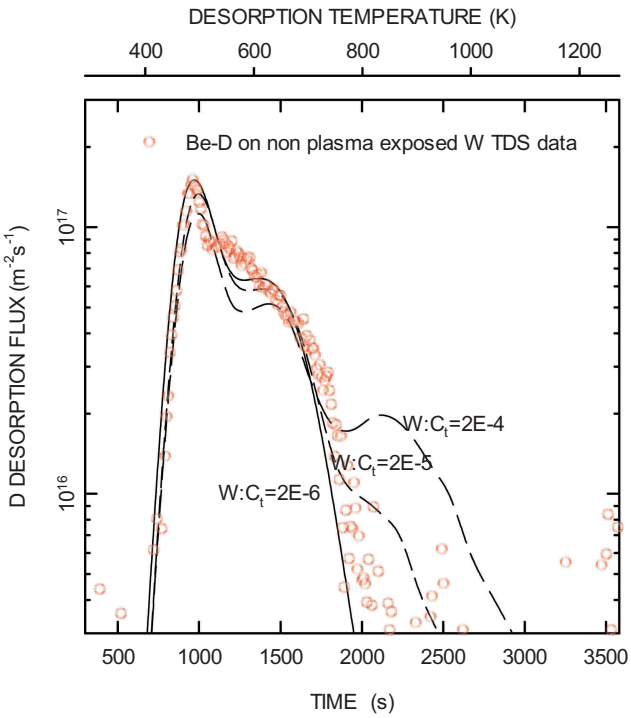

Fig. 5. TDS data for the Be-D codeposit layer on the W sample that was not exposed to plasma (as in Fig. 4) but with TMAP simulations showing the effect of various W substrate intrinsic trap concentrations of 1.6 and 1.9 eV.

using TDS and revealed a notably sharp D release peak at ~630 K and D release corresponding to an areal D retention of $3.8 \pm 0.6 \times 10^{23}$ m^{-2}, which corresponds to a D/Ti ratio of approximately 0.6. Separate samples from the batch were then immersed in a 1.5-kW, 13.56-MHz argon rf plasma in the PISCES-E LPD device. Following plasma immersion, a LIDS pulse of 1100-nm radiation from a 1-kW Coherent Highlight 1000FL fiber laser is applied for a duration of up to 5 s. During the LIDS pulse, the surface temperature profile is measured by a fast two-color pyrometer, and the spectral line emission from Balmer series D-alpha in the plasma is recorded using a fast (1-ms resolution) Avantes four-channel optical spectrometer. The Balmer optical emission in the Ar plasma is representative of the D release from the Ti-D codeposited layer, but the temporal shape of the actual release is modified by the system response due to vacuum pumping and wall recycling. The optical release profiles are then quantified in terms of molecular flow with a separate optical measurement carried out under the same conditions as LIDS but with a calibrated D source leaking into the plasma proximally to the sample location. The system response is obtained from a short burst of D_2 injected into the plasma to approximate an impulse function, and the actual released D is computed by taking the deconvolution of the measured signal and the system response. The integral of the calibrated deconvolution during the LIDS pulse gives the total released D from the sample, which is then easily converted to areal D retention by dividing by the laser-irradiated area. The experimental apparatus is shown schematically in Fig. 6.

Figure 7 shows LIDS data sets for the Ti-D codeposit layer for an irradiated laser spot of 3.5-mm diameter and 0.5-s pulse width. The top row shows the laser power pulse waveform; the middle row shows the fast pyrometer surface temperature measurement; and the bottom row shows the response function of the system, D-alpha emission, and calibrated deconvolution. The columns in Fig. 7 depict three separate laser irradiations of the same sample location. In this sequence of laser shots, increasing laser power was used to obtain full removal of D as demonstrated by the lack of D emission following the second LIDS pulse. When calibrated, the released areal D gives a D retention value of $4.4 \pm 0.9 \times 10^{23}$ m^{-2}. The LIDS measure of D retention is thus found to be in good agreement with that obtained on the control sample measured by conventional TDS. Based on the success of this demonstration, future development of the LIDS system is planned for an in situ measurement of D retention capability on other PISCES LPDs.

VI. LASER-INDUCED BREAKDOWN SPECTROSCOPY FOR IN SITU SURFACE COMPOSITIONAL ANALYSIS

Sputter eroded impurities transported in the SOL plasma in fusion devices can lead to a variety of PMI effects when redeposited. The impurities form mixed materials with the substrate and create layers of codeposits containing hydrogen isotopes and also change the surface morphology, which in turn, then affect the local PMI. Postmortem surface analysis currently provides much of the useful information on these effects, but in situ methods offer the advantage of gaining insight into the dynamic behavior of a material surface during the plasma exposure. Recent experiments in the PISCES laboratory using the technique of laser-induced breakdown spectroscopy (LIBS) have been developed with a specific view toward the technology for studying dynamic PMI in situ.[16] A schematic of the LIBS technology is shown in Fig. 8 for installation on the PISCES-A LPD.

The apparatus utilizes laser radiation from a Q-switched Nd:YAG that produces light of 1064-nm wavelength at pulse widths of ~5 ns. The laser resides

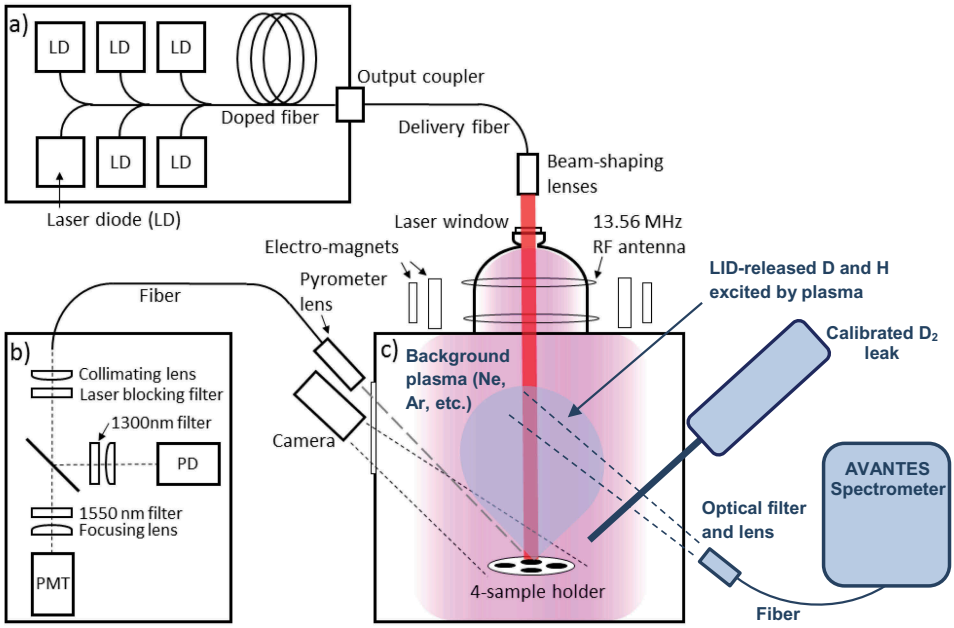

Fig. 6. Schematic representation of LIDS for in situ D retention measurement and removal on the PISCES-E rf LPD.

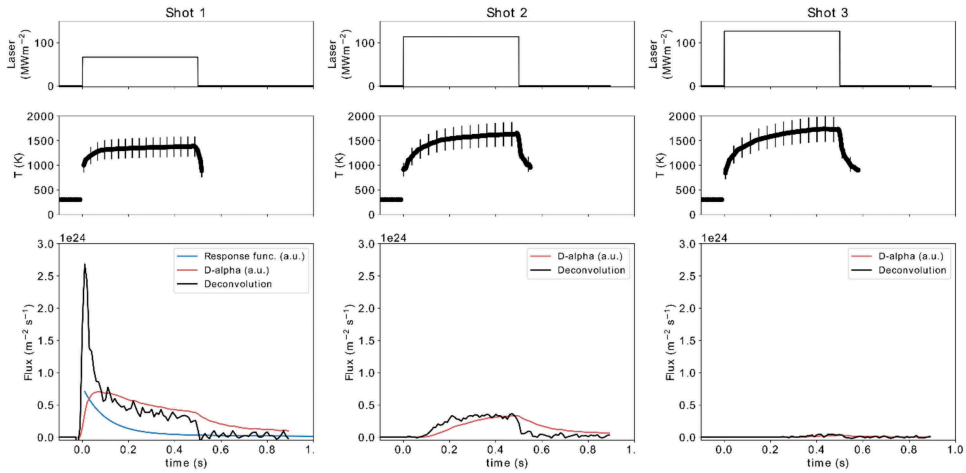

Fig. 7. LIDS data for three sequential 0.5-s laser irradiations of a Ti-D codeposit layer in the same location. Data are shown for laser power pulse waveform (top) and fast pyrometer surface temperature measurement (middle). Bottom panels show the system response function (same for all shots), D-alpha emission, and calibrated deconvolution of the response function and D-alpha. D released corresponds to an areal D retention of $4.4 \pm 0.9 \times 10^{23}$ m^{-2}, which agrees with a conventional TDS measurement on an identical sample of $3.8 \pm 0.6 \times 10^{23}$ m^{-2}.

within an optical safety enclosure with the light beam transported along an optical path utilizing mirrors. Beam entry into PISCES-A is achieved through a focusing lens (FL 750 mm) and standard vacuum window, whereby the beam is then redirected by a further mirror to the PMI target. This mirror is retracted when not in use to minimize contamination of the mirror surface from deposition products from targets. In the current setup the laser energy chosen is ~100 mJ, and the focused spot diameter on the target, determined ex situ, is measured at ~600 μm with a laser confocal microscope (Olympus LEXT OLS4100).

During a LIBS pulse the plasma optical emission near the target is monitored with an echelle-type spectrometer (Andor ME5000) equipped with an intensified charge-coupled-device camera (Andor iStar DH334T) that allows the determination and measurement of radiating species liberated during the laser pulse.

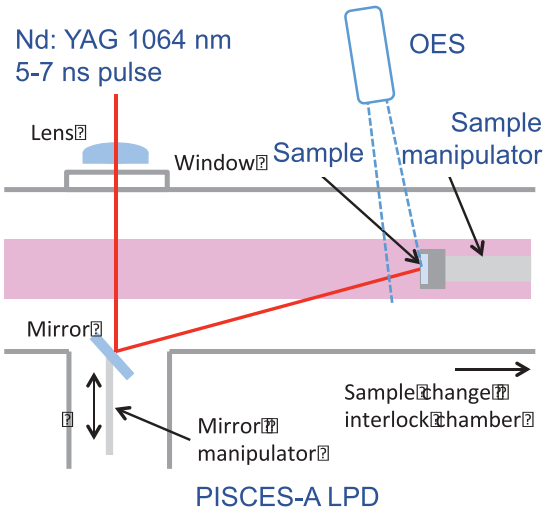

Fig. 8. Schematic representation of LIBS for in situ surface compositional measurement on the PISCES-A LPD.

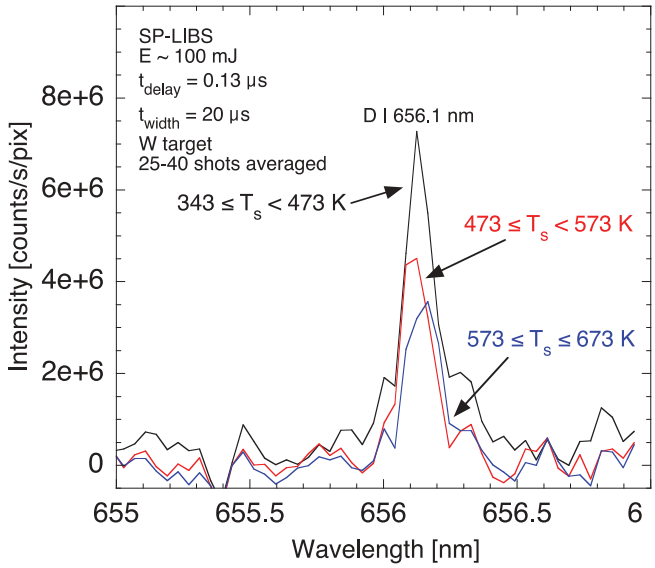

Fig. 9. The Dα (656.1 nm) line emissions measured during LIBS pulse events taken at different sample temperatures on a W sample exposed to D_2 plasma in PISCES A.

Initial experiments with the LIBS diagnostic have focused on measurement of the D retention in W, as demonstrated in Fig. 9, which shows the dependance of Dα (656.1 nm) line emission from LIBS pulse events during D plasma exposure in PISCES A with a plasma of temperature $T_e \sim 6$ eV and density $n_e \sim 6 \times 10^{17}$ m^{-3}. The Dα intensity is a measure of the near-instantaneous dynamic retention in the W surface and is found to decrease with increasing target temperature T_s. An insightful finding in this experiment is that this result is different from what is reported in the literature[17] for D retention in W exposed to high-flux D plasma whereby the retention peaks at 500 to 600 K. The difference is thought to reflect the differences between retention measurements made by in situ LIBS and that reported in Ref. 17, which is a compilation of D in W retention data determined by the techniques of TDS and NRA. LIBS is entirely surface sensitive, probing the top few hundred nanometers, whereas TDS and NRA are considerably more bulk D sensitive by comparison. Indeed, the depth probed in the surface is ~110 nm for the LIBS system described, while the whole sample thickness is measured in TDS, and many microns are probed in typical analysis of D in W by NRA (Ref. 17). Further, the peak in D retention at ~500 to 600 K is thought to be associated with the formation of blisters that are usually seen at depths much beyond the LIBS measurement range.[18] Ongoing research with the PISCES LIBS system is planned for development of the technology into an in situ measurement capability for D retention and surface composition. Complete details for this study are to be found in Ref. 16.

VII. SUMMARY

Current and continuing research at the PISCES laboratory at UCSD is a focused mix of experimental science in basic PMI and boundary plasma studies with emphasis given to technology development when appropriate to the PISCES scientific mission. PISCES researchers and engineers carry out this mission utilizing a host of plasma facilities and material diagnostic methods to aid in the testing of hypotheses through experiment, theory, and modeling that, in turn, allows for the projection of PMI performance under fusion-relevant conditions. The work summarized here is a selection of current PISCES experiments and technology development efforts with a view to supporting the needs of ITER and U.S. fusion nuclear science initiatives, which were presented and discussed at the 23rd TOFE topical meeting.

ACKNOWLEDGMENTS

This work is supported by U.S. Department of Energy grant award numbers DE-FG02-07ER54912, DE-SC001-8281, and DE-SC001-8268.

FUNDING

This work is supported by a USDOE Grant Awards: #DE-FG02-07ER54912, #DE-SC001-8281, and #DE-SC001-8268.

ORCID

M. J. Baldwin http://orcid.org/0000-0001-6335-2255

References

1. R. MAINGI et al., "Fusion Energy Sciences Workshop on Plasma Materials Interactions: Report on Science Challenges and Research Opportunities in Plasma Materials Interactions," Princeton Plasma Physics Laboratory (2015); https://www.osti.gov/biblio/1414414-fusion-energy-sciences-workshop-plasma-materials-interactions-report-science-challenges-research-opportunities-plasma-materials-interactions.
2. D. M. GOEBEL, G. CAMPBELL, and R. W. CONN, "Plasma Surface Interaction Experimental Facility (PISCES) for Materials and Edge Physics Studies," *J. Nucl. Mater*, **121**, 277 (1984); https://doi.org/10.1016/0022-3115(84)90135-1.
3. Y. HIROOKA et al., "A New Plasma-Surface Interactions Research Facility: PISCES-B and First Materials Erosion Experiments on Bulk-Boronized Graphite," *J. Vac. Sci. Technol. A*, **8**, 1790 (1990); https://doi.org/10.1116/1.576805.
4. R. P. DOERNER and C. MAYS, "Beryllium Dust Generation Resulting from Plasma Bombardment," *Fusion Eng. Des.*, **37**, *2*, 325 (1997); https://doi.org/10.1016/S0920-3796(97)00069-0.
5. K. D. HAMMOND, "Helium, Hydrogen, and Fuzz in Plasma-Facing Materials," *Mater. Res. Express*, **4**, 104002 (2017); https://doi.org/10.1088/2053-1591/aa8c22.
6. R. P. DOERNER et al., "Motion of W and He Atoms During Formation of W Fuzz," *Nucl. Fusion*, **58**, 066005 (2018); https://doi.org/10.1088/1741-4326/aab96a.
7. M. THOMPSON et al., "Observation of a Helium Ion Energy Threshold for Retention in Tungsten Exposed to Hydrogen/Helium Mixture Plasma," *Nucl. Fusion*, **56**, 104002 (2016); https://doi.org/10.1088/0029-5515/56/10/104002.
8. T. PETTY et al., "Tungsten 'Fuzz' Growth Re-Examined: The Dependence on Ion Fluence in Non-Erosive and Erosive Helium Plasma," *Nucl. Fusion*, **55**, 093033 (2015); https://doi.org/10.1088/0029-5515/55/9/093033.
9. G. LONGHURST, "TMAP7 User Manual," INEEL/EXT-04-02352, Rev. 2, Idaho National Engineering and Environmental Laboratory (2008).
10. M. J. SIMMONDS et al., "Expanding the Capability of Reaction-Diffusion Codes Using Pseudo Traps and Temperature Partitioning: Applied to Hydrogen Uptake and Release from Tungsten," *J. Nucl. Mater.*, **508**, 472 (2018); https://doi.org/10.1016/j.jnucmat.2018.05.080.
11. V. K. ALIMOV, J. ROTH, and S. LINDIG, *At. Plasma Mater. Interact. Data Fusion*, **15**, 3 (2012).
12. M. J. BALDWIN and R. P. DOERNER, "Hydrogen Isotope Transport Across Tungsten Surfaces Exposed to a Fusion Relevant He Ion Fluence," *Nucl. Fusion*, **57**, 076031 (2017); https://doi.org/10.1088/1741-4326/aa70b1.
13. L. GAO et al., "Deuterium Supersaturation in Low-Energy Plasma-Loaded Tungsten Surfaces, *Nucl. Fusion*, **57**, 016026 (2017).
14. M. J. BALDWIN, T. SCHWARZ-SELINGER, and R. P. DOERNER, "Experimental Study and Modelling of Deuterium Thermal Release from Be–D Co-Deposited Layers," *Nucl. Fusion*, **54**, 073005 (2014); https://doi.org/10.1088/0029-5515/54/7/073005.
15. J. H. YU, M. J. BALDWIN, M. J. SIMMONDS, and A. ZALOŽNIK, "Time-Resolved Laser-Induced Desorption Spectroscopy (LIDS) for Quantified *In-Situ* Hydrogen Isotope Retention Measurement and Removal from Plasma Facing Materials," *Rev. Sci. Instrum.*, **90,** 073502 (2019); https://doi.org/10.1063/1.5100162.
16. D. NISHIJIMA, M. PATINO, and R. P. DOERNER, "Development of a LIBS System for In Situ Surface Measurements During Plasma Exposure in PISCES-A," *Rev. Sci. Instrum.*, **89**, 10J105 (2018); https://doi.org/10.1063/1.5034349.
17. M. J. BALDWIN et al., "Effect of He on D Retention in W Exposed to Low-Energy, High-Fluence (D, He, Ar) Mixture Plasmas," *Nucl. Fusion*, **51**, 103021 (2011); https://doi.org/10.1088/0029-5515/51/10/103021.
18. M. H. J. 't HOEN et al., "Surface Morphology and Deuterium Retention of Tungsten After Low- and High-Flux Deuterium Plasma Exposure," *Nucl. Fusion*, **54**, 083014 (2014); https://doi.org/10.1088/0029-5515/54/8/083014.